Morphologies and phase diagrams of ABC star triblock copolymers confined in a spherical cavity

ARTICLE *in* SOFT MATTER · APRIL 2013

Impact Factor: 4.03 · DOI: 10.1039/C3SM27770D

Soft Matter

RSC Publishing

PAPER

View Article Online
View Journal | View Issue

Morphologies and phase diagrams of ABC star triblock copolymers confined in a spherical cavity

Cite this: *Soft Matter*, 2013, **9**, 4843

Shiben Li,*[ab] Ying Jiang[ab] and Jeff Z. Y. Chen[b]

The morphologies and phase diagrams exhibited by symmetric ABC star triblock copolymer nanoparticles are investigated by using the real-space self-consistent field theory. A variety of three-dimensional morphologies, such as spherically concentric lamellae and ring-like structures, are identified in the triangular phase diagrams for the polymeric nanoparticles, depending on the volume fractions of the components and the interaction between the polymers and the confining spherical surface. We first study a number of examples where the confining radius and degree of interactions between the polymer and the spherical surface are fixed. A neutral surface that has no energetic preference on any ABC component induces ring-like structures in axisymmetry in an orbicular region of the phase diagram, which surrounds the central region where distorted cylinder phases are stable; a spherical surface that attracts one of the three polymer components induces distorted cylinders into the ring-like structures in a central region of the phase diagram; a spherical surface that repels one of the components stabilizes a lamella-like structure in spherical symmetry in a large region of the phase diagrams. We then focus on an example of polygonal tiling morphologies to study the effects due to variations of the spherical radius and the degree of interactions between the polymer and the spherical surface. The results show that the degree of interactions can obviously influence the formation of morphologies but the spherical radius only affects the polygonal tiling morphologies through slightly adjusting their natural arrangement in the neutral surface case.

Received 30th November 2012
Accepted 6th March 2013

DOI: 10.1039/c3sm27770d

www.rsc.org/softmatter

I Introduction

Block copolymer nanoparticles made of various structures have wide applications in several areas, such as drug delivery, optical data storage, and spherical dielectric resonators.[1–4] For example, core–shell block copolymer nanoparticles containing different dyes in the core and shell may be used as periodic recording media for optical data storage with greater power and versatility than binary data storage devices.[2] Theoretically, a spherical nanoparticle is commonly modeled by a polymer melt confined in a spherical cavity. The physical properties of these polymer nanoparticles are not only closely related to their confinement conditions but also influenced by the molecular architectures of the polymers. The surface interaction and competition between the domain size of an ordered bulk structure and the confinement dimension can yield a diverse range of morphologies in different symmetries, as previously demonstrated in systems made of linear AB diblock copolymers.[5,6] Exploration of novel morphologies and the corresponding phase behavior of block copolymers with complex topologies in nanoparticles can provide a rich library of templates that can be used for potential practical applications.

An ABC star triblock copolymer possesses a special topology in which the ends of three blocks are linked at one junction point. Such copolymers exhibit several unique morphologies in bulk, which are absent in their ABC linear counterparts. Some striking examples include polygonal tiling (PT) patterns that have junction points arranged in straight lines, and display a columnar structure with polygonal cross sections.[7,8] The PT patterns exhibit two-dimensional periodicity, which were observed by transmission electron microscopy (TEM) and small-angle X-ray scattering (SAXS) in various polymer systems[9–17] and reproduced in modeling efforts, including Monte Carlo (MC) simulations, self-consistent field theory (SCFT), and dissipative particle dynamics simulations.[7,18–23] In these studies, triangular phase diagrams were constructed to examine the phase behavior of the observed morphologies, especially those of PT. ABC star triblock copolymers are candidates for forming hierarchical structures due to the geometric restriction presented by their junction points.[7,20,24,25] These hierarchical morphologies include hierarchical lamellae (HLs), cylinders-in-lamellae, lamellae-in-cylinders, and lamellae-in-spheres. By comparing their free energies, the relative stabilities of HLs may be analyzed and

[a]*Department of Physics, Wenzhou University, Wenzhou, Zhejiang 325035, China. E-mail: shibenli@wzu.edu.cn*

[b]*Department of Physics and Astronomy, University of Waterloo, Waterloo, Ontario, Canada, N2L 3G1*

tuned *via* the interactions among the three blocks.[25] Experimental investigations revealed that morphological transitions among cylinders-in-lamellae, lamellae-in-cylinders, and lamellae-in-spheres can occur by changing the length of a single block.[24]

Few studies have been conducted on confined ABC star triblock copolymers, in contrast to confined diblock copolymers, which are well-studied.[26] Earlier MC simulations concentrated on the conformational properties of ABC star triblock copolymer thin films.[27–31] The distance between two confining surfaces as well as the chain length of star-branched polymer chains were varied to investigate their mean-square center-to-center distance, mean-square radius of gyration, longest relaxation time, and diffusion dynamics.[27,29] The properties of ABC star triblock copolymer thin films were compared with their linear counterparts, and results showed that these properties of star-branched chains are minimally affected by confinement.[31] Two SCFT studies were recently carried out on nearly symmetric ABC star triblock copolymer thin films with preferential and neutral surfaces.[32,33] By varying the film thickness and the strength of the surface fields, a variety of morphologies were identified and the phase behavior of ABC star triblock copolymers was evaluated in triangular phase diagrams. A pore geometry provides a two-dimensional confinement that enables the polymer chains to frustrate in two directions while to comparatively relax in the third direction. A SCFT study was carried out to investigate how HLs self-assemble into pore geometries with preferential surfaces;[34] results showed that when the pore diameter is not excessively large bulk HL may be distorted into concentric arrangements in the outer region of a pore while an irregular core appears in the central region. A MC investigation on a system of $A_6B_6C_6$ star triblock copolymers was carried out to examine how PT structures are frustrated in cylindrical nanopores, and a variety of novel structures were reportedly obtained by varying the pore diameter.[35] Very recently, a SCFT study was performed for ABC star triblock copolymers inside a pore that has a neutral surface. A series of novel nanostructures were identified in the triangular phase diagrams constructed by three volume fractions.[36] The transitions between these phases appear to be of the first-order type, as such stable phases can be distinguished from metastable ones by a comparison of their free energies.

The nanoparticle boundary condition requires the presence of a confining spherical surface; this means that there exist typical frustrations of the bulk morphologies in all directions. Such a confinement introduces a tendency to make either a concentric structure as the surface prefers to attract the confined polymers, or the perpendicular lamellae as the surface is neutral, in the lamella-forming diblock copolymer nanoparticles.[37,38] The spherical confinement also produces several novel morphologies for cylinder-forming diblock copolymers when the confining diameter is not commensurate to the bulk repeat period.[26,39]

Inspired by these earlier studies, in this paper we aim at exploration of the morphologies of ABC star triblock copolymer nanoparticles and their phase behavior in the parameter space. A SCFT treatment, numerically implemented by a pseudospectral method based on the parallel fast Fourier transformation technique, is used to calculate the structure of ABC star triblock copolymers by adding interaction energies with the confinement surface. A number of different scenarios are examined here: neutral surface and surface that has a typical attractive or repulsive interaction with the polymer components. For simplicity, we focus on triblock copolymers having the same Flory–Huggins interaction between the three components.

II Theoretical method

A Formalism

We consider a system of n star triblock copolymers confined in a spherical cavity. Each star triblock copolymer has a degree of polymerization N and consists of three branches with distinctive chemical compositions, respectively labeled A, B, and C. The volume fractions of A, B, and C monomers are f_A, f_B and f_C, respectively, and the statistical segment length of the polymer is assumed to be a. The masking technique, previously proposed by Fredrickson *et al.*,[40] is used to realize the spherical confinement effects. In the masking technique, an interfacial density function $\phi_W(\mathbf{r})$ is imposed, which expels the ABC polymer segments into the spherical cavity, following a modified incompressibility constraint,

$$\phi_A(\mathbf{r}) + \phi_B(\mathbf{r}) + \phi_C(\mathbf{r}) + \phi_W(\mathbf{r}) = 1, \quad (1)$$

where $\phi_i(\mathbf{r})$ represents the volume fraction of species i (i = A, B, C). Physically, the region where $0 < \phi_W(\mathbf{r}) < 1$ represents overlap of the surface with ABC polymers; those where $\phi_W(\mathbf{r}) = 0$ and $\phi_W(\mathbf{r}) = 1$ define the regions of an ABC polymer mixture and the impenetrable hard wall, respectively. This means that the selection of $\phi_W(\mathbf{r})$ determines the geometry of the confinement. Here, to model a spherical cavity we consider using a cosine function for $\phi_W(r)$,

$$\phi_W(r) = \begin{cases} 1 & r > R \\ \frac{1}{2}\left\{1 + \cos\left[\frac{\pi}{T}(R - r)\right]\right\} & R - T \le r \le R \\ 0 & R - T > r \end{cases}, \quad (2)$$

where r is the distance from the central point of the confinement, R the spherical radius, and T the wall thickness. A hyperbolic tangent function was employed to realize the film geometry in previous works.[32,40] It turns out that the exact function form of the confinement function does not influence the main results presented in this paper, as long as there is a relatively sharp interface represented by a small T. The clear advantage of this interface, controlled by an interface thickness T, is the avoidance of potential numerical divergence seen in models containing a sharp surface profile. The results presented below are obtained by using $T = 0.1R$. We can then write the standard SCFT free energy per polymer to include a sum of quadratic terms in the form $\phi_i(\mathbf{r})\phi_W(\mathbf{r})\chi_{iW}$,[40,41]

$$\frac{F}{nk_BT} = -\ln\left(\frac{Q}{V}\right) + \frac{1}{V}\int d\mathbf{r}(\chi_{AB}N\phi_A\phi_B + \chi_{BC}N\phi_B\phi_C + \chi_{AC}N\phi_A\phi_C) + \frac{1}{V}\int d\mathbf{r}(\chi_{AW}N\phi_A\phi_W + \chi_{BW}N\phi_B\phi_W + \chi_{CW}N\phi_C\phi_W) - \frac{1}{V}\int d\mathbf{r}(w_A\phi_A + w_B\phi_B + w_C\phi_C) - \frac{1}{V}\int d\mathbf{r}\eta(1 - \phi_A - \phi_B - \phi_C - \phi_W), \quad (3)$$

where the Flory–Higgins parameter χ_{ij} controls the incompatibility degrees between different species i and j, and χ_{iW} indicates the dimensionless measure of the surface interaction between species i and the spherical wall. Phenomenologically, $\chi_{iW} = 0$ corresponds to a neutral polymer–surface interaction, $\chi_{iW} < 0$ represents a wall surface attracting the i-type monomers, and $\chi_{iW} > 0$ represents a wall surface repelling the i-type monomers. In the above expression, $\eta = \eta(\mathbf{r})$ is the Lagrange multiplier introduced to incorporate the incompressibility condition and V represents the effective volume occupied by the copolymers, $V = \int d\mathbf{r}[1 - \phi_W(\mathbf{r})]$. The effective diameter can be calculated according to the formula, $V = \frac{1}{6}\pi d_{eff}^3$. According to eqn (2), d_{eff} is comparable to but smaller than $2R$. The partition function of a single triblock copolymer, Q, will be defined below.

The architecture of a star triblock polymer contains a central branching point that we label $s = 0$. Along each branch, we can label the monomers by an arc variable s, where $0 \le s \le f_i$. Of central concern in SCFT is the calculation of the probability $q_i^+(\mathbf{r},s)$ for a polymer portion starting from the f_i-th terminal anywhere in space and ending with the terminal s located in $\mathbf{r}$. This probability, also called propagator in SCFT, follows modified diffusion equation (MDE),

$$-\frac{\partial q_i^+(\mathbf{r},s)}{\partial s} = R_g^2\nabla^2 q_i^+(\mathbf{r},s) - w_i(\mathbf{r})q_i^+(\mathbf{r},s), \quad (4)$$

with the initial condition

$$q_i^+(\mathbf{r},f_i) = 1,$$

where $w_i(\mathbf{r})$ is the mean field that the i-type monomers experience, produced by the surrounding chains. In eqn (4), $R_g^2 = \frac{1}{6}Na^2$ is the mean-square gyration radius of an ideal linear Gaussian chain. A complementary propagator, $q_i(\mathbf{r},s)$, is needed to complete the calculation of the partition function. This propagator represents the probability of finding the polymer portion starting from the branching point $s = 0$ anywhere in space and ending with the terminal s located in $\mathbf{r}$ and satisfies

$$\frac{\partial q_i(\mathbf{r},s)}{\partial s} = R_g^2\nabla^2 q_i(\mathbf{r},s) - w_i(\mathbf{r})q_i(\mathbf{r},s). \quad (5)$$

This equation is supplemented by the initial condition

$$q_i(\mathbf{r},0) = q_j^+(\mathbf{r},0)q_k^+(\mathbf{r},0)$$

where $(i, j, k) = (A, B, C)$, (B, C, A) or (C, B, A). The partition function Q in eqn (3) is for a single polymer chain, which can then be calculated from

$$Q = \int q_i(\mathbf{r},f_i)d\mathbf{r}, \quad (6)$$

where f_i can be any one of f_A, f_B, and f_C.

Minimizing the free energy in eqn (3) with respect to w_A, w_B, and w_C gives the local monomer volume fractions,

$$\phi_A(\mathbf{r}) = \frac{V}{Q}\int_0^{f_A} ds q_A(\mathbf{r},s)q_A^+(\mathbf{r},s), \quad (7)$$

$$\phi_B(\mathbf{r}) = \frac{V}{Q}\int_0^{f_B} ds q_B(\mathbf{r},s)q_B^+(\mathbf{r},s), \quad (8)$$

and

$$\phi_C(\mathbf{r}) = \frac{V}{Q}\int_0^{f_C} ds q_C(\mathbf{r},s)q_C^+(\mathbf{r},s). \quad (9)$$

Minimization of the free energy per chain, eqn (3), with respect to ϕ_A, ϕ_B, and ϕ_C leads to expressions for the external fields,

$$w_A(\mathbf{r}) = \chi_{AB}N\phi_B(\mathbf{r}) + \chi_{AC}N\phi_C(\mathbf{r}) + \chi_{AW}N\phi_W(\mathbf{r}) + \eta(\mathbf{r}), \quad (10)$$

$$w_B(\mathbf{r}) = \chi_{AB}N\phi_A(\mathbf{r}) + \chi_{BC}N\phi_C(\mathbf{r}) + \chi_{BW}N\phi_W(\mathbf{r}) + \eta(\mathbf{r}), \quad (11)$$

and

$$w_C(\mathbf{r}) = \chi_{AC}N\phi_A(\mathbf{r}) + \chi_{BC}N\phi_B(\mathbf{r}) + \chi_{CW}N\phi_W(\mathbf{r}) + \eta(\mathbf{r}). \quad (12)$$

Eqn (4)–(12) are considered self-consistently in SCFT for the calculation of ϕ_i, w_i and Q, which is usually tackled by a numerical approach.

B Numerical approach

One of the main steps is to solve the MDE, eqn (4) and (5) numerically, step by step in s, for given fields w_i. Numerically, these equations were solved in the framework of a pseudo-spectral (PS) scheme, which is unconditionally stable and has the second-order accuracy in contour step length, $(\Delta s)^2$.[42] Because of the spherical confinement, the $\mathbf{r}$-dependence is dealt with in real space rather than in the Fourier space which would be more suitable for a periodic system otherwise.

The overall strategy follows the combinatorial screening method originally proposed by Drolet and Fredrickson.[18,43] Once the external fields are given, the volume fraction, Q, and the free energy can be obtained from solving the MDEs. In this method, a relaxation process is assumed, starting with an initially guessed mean field. The relaxation steps are repeated until the relative difference between the free energies of the sequential iteration steps is reduced to the pre-specified precision. In this work, we took a convergence criterion such that the difference of the free energies per chain, eqn (3), from two consecutive iterations is less than 10^{-6}.

Due to the extensiveness of the three-dimensional computation, the numerical algorithm was parallelized, which enabled implementation on a distributed-memory computer cluster,

similar to the procedure used in a previous work.[44] In the calculations for the bulk properties, the periodic boundary conditions in all three Cartesian directions were introduced in the PS solution to MDEs. One additional parameter for a periodic structure is the domain size, which was optimized by adjusting the simulation-box lengths in all three directions, in order to minimize the free energy.

All results presented below were obtained by setting $\Delta s = 0.0025$. The computational grid system in the three-dimensional space contained 64 sites in each direction; the grid spacing in three directions, Δx, Δy, and Δz, was set to a value ranging from $0.06R_g$ to $0.21R_g$ for the calculation of the bulk structure and $\Delta x = \Delta y = \Delta z = 0.15R_g$ for the calculation of the confined case. These values were adopted by trial and error and for the current problem it efficiently produced a morphology that corresponds to a local free energy minimum.

Because the search for free energy minima was performed by a downhill algorithm, for every specified point in the parameter space we might obtain different local energy minima, depending on the initial conditions. In this work, we take the structure with the lowest free energy as the most stable phase, selected from all structures produced by proposing twenty different initial guesses of the mean fields. A disclaimer must be made that the obtained structure does not necessarily correspond to the absolute global minimum.

III Results and discussion

Generally, the type of morphologies obtained by applying SCFT depends on the physical parameters used in our model: f_i, $\chi_{ij}N$, $\chi_{iW}N$, and d_{eff}, where i = A, B and C. A complete description of the morphologies in the entire parameter space, however, is formidable. In this section, we examine several subsets of phase diagrams, selected from a number of representative values of these parameters. To focus on the influence of the compositions on the phase behavior, we consider symmetric ABC star polymers,

$$\chi_{AB}N = \chi_{BC}N = \chi_{AC}N = 40. \quad (13)$$

At these values the system is already in a microphase-separated regime.[20] According to a previous study, the system reported here is located in the intermediate segregation region between weak and strong segregation.[33] In the following, we start with the discussion of the simplest case, the phase diagram of symmetric ABC triblock copolymers in bulk (*i.e.*, without the spherical confinement). We then explore the effects of a neutral spherical confinement on the phase diagram by selecting a specific d_{eff}. The d_{eff} is chosen as about twice as the bulk periods, which is suitable to observe the phase behaviors, as demonstrated in the diblock copolymer nanoparticles.[39] The effects of attraction and repulsion between the confinement walls and the block copolymers on the morphology are described in the following subsections, again by a fixed d_{eff}. Finally, the cases on the effects of changing d_{eff} and $\chi_{iW}N$ are examined.

In a three-component mixture system, one customarily describes the phase behavior by means of the tertiary phase diagram where the overall volume fractions f_A, f_B, and f_C label each side of a triangle. We use this as the main tool to classify the morphology observed in this work, aided by plotting examples of real-space three dimensional structures in color; red, green, and blue illustrate the A-rich, B-rich, and C-rich regions in space, respectively. To demonstrate the inner structures more clearly, in some cases every color is separately plotted.

A Bulk structure without confinement

For the bulk properties with fixed $\chi_{ij}N = 40$, the only set of free parameters is (f_A, f_B, f_C) where $f_A + f_B + f_C = 1$. Our computer algorithm solves SCFT in a full three-dimensional (3D) space, which no doubt is needed as the reference for the confined structures described below. Within a $\Delta f = 0.1$ grid system for every f_i, out of 36 different sets of (f_A, f_B, f_C), only 8 sets are symmetrically independent. Their structures are illustrated in Fig. 1; the other 28 derived structures are shown in Fig. 2. The eight main bulk structures studied in this work all display translational symmetries along one or two directions, maintaining a periodic structure in the other two or one directions, as illustrated by the left panels of Fig. 1(a)–(h). The periodic structures are further plotted on the right panels, showing the basic lattice structures that can be described by constants L_1 and L_2 for a two-dimensional (2D) periodic structure, and L_1 for a one-dimensional (1D) periodic structure. The free energy per chain for these structures, together with L_1 and L_2, are presented in Table 1.

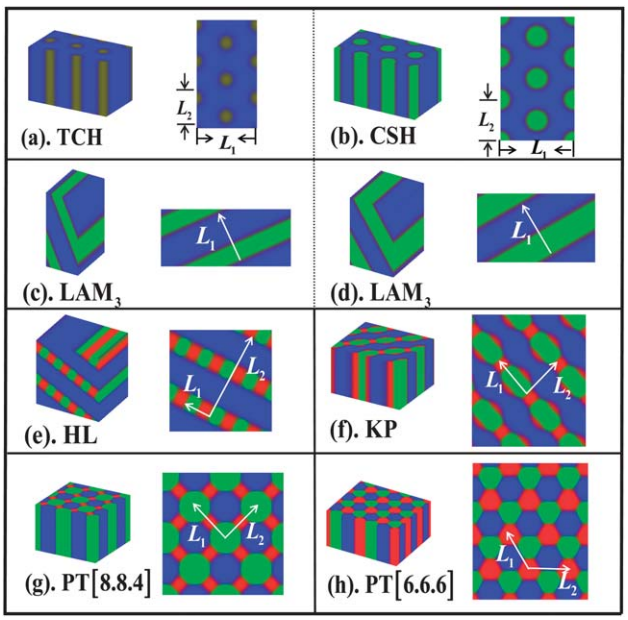

Fig. 1 Bulk morphologies of symmetric ABC star triblock copolymers obtained from the current work for $\chi_{AB}N = \chi_{BC}N = \chi_{AC}N = 40$. Red, green and blue colors represent A-, B- and C-rich domains, respectively. The structures correspond to volume fractions (f_A, f_B, f_C) specified in the third column of Table 1.

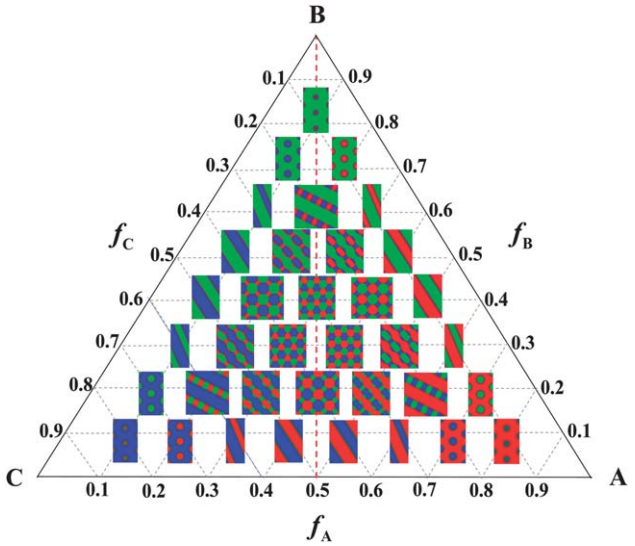

Fig. 2 Triangular phase diagram of ABC star triblock copolymers in bulk. Structures are arranged in (f_A, f_B, f_C). The red dashed line is the isopleth of the AC boundary.

A careful examination of the 8 structures in Fig. 1 reveals that they belong to 6 independent crystallographic groups. The first group is the two hexagonal columnar structures, the two-colored hexagonal (TCH) and core–shell hexagonal (CSH) columns in Fig. 1(a) and (b), which have a 6-fold symmetry normal to the translational-symmetry direction. The 9 columnar structures occupy the corners of the tertiary phase diagram in Fig. 2; the major component provides a background where the minority component aggregates within the approximately cylindrical columns which have surfaces decorated by the component with the lowest volume fraction. The second group is the two three-color lamellar (LAM_3) structures in Fig. 1(c) and (d) that have translational symmetries in two directions. These two LAM_3 have different periodicities, listed in Table 1. The 12 lamellar structures occupy the edges of the tertiary phase diagram. The two major components form alternating lamellar bands while the minority component is sandwiched between these bands. These two structures, columns and lamallae, can be traced back to structures found in diblock copolymers, where one of the three arms in the current model disappears.

The third typical structure, hierarchical lamella (HL), is displayed in Fig. 1(e), consisting of lamellar bands of the major component, and mixed bands of the two minor components. Due to the branching symmetry in a star polymer, the two neighboring minority bands have an alternative arrangement along the plane direction normal to the lamellar axis. The 3 HL structures occupy the near-corner region of the tertiary phase diagram in Fig. 2. Next to HL, emerges the knitting pattern (KP) structure shown in Fig. 1(f); the major and next-to-major components form a layered system, with the minor component knitting between the layers. The phase diagram in Fig. 2 contains 6 KP structures. The KP structure reported here agrees with a previous SCFT study on ABC star triblock copolymers, having the same volume fraction but different interaction parameters, $\chi_{ij}N = 32$ and 35.[20,36] This indicates that KP is stable over a relatively wide range of $\chi_{ij}N$. The last two polygonal tiling (PT) structures, PT [6.6.6] and [8.8.4], arise in a region where the three components have comparable overall volume fractions. These are columnar structures, in which each of the three components aggregates to form columns; in the plane normal to the column direction, the pattern contains 4-fold (*i.e.*, PT [8.8.4]) or 6-fold (*i.e.*, PT [6.6.6]) rotational symmetries. The central region of the phase diagram in Fig. 2 is occupied by PT structures. The pattern in cross sections of the PT structures identifies the subset, [*k*, *l*, *m*], where a *k*-gon, *l*-gon, and *m*-gon meet consecutively at each vertex. These two tiling patterns were observed in SCFT simulations where $\chi_{ij}N = 35$,[20] and in the various experimental systems by TEM and SAXS,[11–16] and then reproduced in recent SCFT studies with $\chi_{ij}N = 30$, 32 and 60.[22,23,36] Our results are in agreement with these previous results. However, we have now confirmed that these structures are stable in a full 3D study, in comparison with the approach taken in ref. 14 and 17 where the 2D version of MDE was used.

The triangular phase diagram itself, shown in Fig. 2, contains mirror symmetries about three isopleths. This is due to the symmetric triblock copolymers considered here, through eqn (13) and their special star architecture. The phase diagram symmetry is a common feature that has been noted previously with different degrees of incompatibility.[20,22,36] This can be contrasted with the ABC linear architecture where only a mirror symmetry about the isopleth normal to the AC side appears in the triangular phase diagram.[45] At the compositions specified in

Table 1 The composition (f_A, f_B, f_C), minimized free energy per chain, and characteristic periodicities L_1 and L_2 of the structures in Fig. 1, listed according to the label in the same figure. Estimated numerical errors are presented in subscript next to the corresponding digit

Morphology		Composition (f_A, f_B, f_C)	Saddle point free energy ($/nk_BT$)	Bulk period ($/R_g$)	
				L_1	L_2
(a)	TCH	(0.1,0.1,0.8)	$6.58112 \pm_3$	$6.16 \pm_5$	$3.54 \pm_8$
(b)	CSH	(0.1,0.2,0.7)	$7.6271 \pm_3$	$7.31 \pm_6$	$4.25 \pm_9$
(c)	LAM_3	(0.1,0.3,0.6)	$7.8726 \pm_5$	$4.27 \pm_6$	
(d)		(0.1,0.4,0.5)	$7.90436 \pm_1$	$4.58 \pm_6$	
(e)	HL	(0.2,0.2,0.6)	$9.10388 \pm_5$	$2.07 \pm_1$	$7.55 \pm_1$
(f)	KP	(0.2,0.3,0.5)	$9.5859 \pm_6$	$4.40 \pm_9$	$4.41 \pm_9$
(g)	PT [8.8.4]	(0.2,0.4,0.4)	$9.5790 \pm_8$	$4.21 \pm_6$	$4.20 \pm_7$
(h)	PT [6.6.6]	(0.3,0.3,0.4)	$9.9343 \pm_8$	$4.01 \pm_9$	$4.00 \pm_9$

Table 1, we did not find any other structures, in particular, other 3D structures with no translational symmetries. In view of the fact that in a diblock copolymer mixture, a special case of triblock copolymers where the volume fraction of one component is absent, there exist full 3D bcc and gyroid structures,[46] we expect that the small region near CSH may correspond to the core–shell bcc structures. A previous work also reported several hierarchical structures of non-translational symmetries for ABC star triblock copolymers with symmetric incompatibility degrees, indicating that not all phases have translational symmetries in the phase diagram.[7] The results suggest that the phases having cubic and other symmetries may emerge when the phase diagrams are refined in smaller steps of volume fractions. The phase diagram in Fig. 2 needs to be refined but this is not the central focus of the current paper.

B Spherical cavity with neutral walls

In this section we discuss the main features of the morphologies of ABC triblock copolymers confined in a spherical cavity of diameter

$$d_{\text{eff}} = 7.10R_{\text{g}}, \tag{14}$$

where the cavity surface is neutral to the confined polymers and only acts as an excluding wall. In our model, we set

$$\chi_{\text{AW}}N = \chi_{\text{BW}}N = \chi_{\text{CW}}N = 0, \tag{15}$$

and consider various sets of $(f_{\text{A}}, f_{\text{B}}, f_{\text{C}})$ in an increment of $\Delta f = 0.1$. Right away, we realize that due to the symmetry of the system, the 36 sets of $(f_{\text{A}}, f_{\text{B}}, f_{\text{C}})$ only contain 8 independent structures, shown in Fig. 3.

The 8 morphologies in Fig. 3 can be divided into three groups based on their 3D patterns described below.

(a)–(c): Distorted cylinder (DC) structures. These structures are similar to those reported earlier in diblock copolymers.[37,39] Our tertiary system contains a pattern where the majority component provides a background for the minority structure to interweave; the interface between the core minority structure and the background is coated with monomers of the lowest volume fraction. Typical examples are shown in Fig. 3(a)–(c). As the overall volume fraction of the minority component increases and more monomers become available, the minority structures are more connected. The structure in (c) sits on the parameter set, $(f_{\text{A}}, f_{\text{B}}, f_{\text{C}}) = (0.1, 0.3, 0.6)$, which corresponds to a lamellar phase in the bulk system (see Fig. 2) where $d_{\text{eff}} = \infty$. As d_{eff} is adjusted down to $7.10R_{\text{g}}$, the connection with the original LAM structure might have yielded to a DC structure.

(d)–(f): Mushroom ring (MR), hierarchical disk (HD), and three-colored ring (TCR) structures. Going to the middle of the edge of the phase diagram in Fig. 4, we observed two MR structures, originated from the LAM_3 structure in a bulk. The spherical cavity cuts the layered structure, and makes minor modifications in the near-wall region. Because of the incompatible geometries here, the entire confined structure resembles a mushroom shape, maintaining an axial symmetry, as shown in Fig. 3(d). Minority-block domains are embedded between the interfaces of the mushroom and ring structures. The MR structure is similar to those reported in diblock copolymer nanoparticles.[38] HD occurs in the phase diagram with $(f_{\text{A}}, f_{\text{B}}, f_{\text{C}}) = (0.2, 0.2, 0.6)$, where originally the HL structure is stable in the bulk phase diagram. HD resembles a spherical cutout from HL, shown in Fig. 3(e). It possesses an axial symmetry and includes two parallel disks formed by majority-blocks and a hierarchical disk originating from the bulk HL. The three-colored ring (TCR) occurs in the original phase diagram where KP structure is stable in the bulk phase. In the axisymmetric TCR, all three components form concentric ring-like structures, where the major component assembles into two parallel rings and other components transit into the ring in small disks. TCR is continuously connected to the adjacent MR; KP, or its derivative remnant in spherical confinement disappears from the phase diagram.

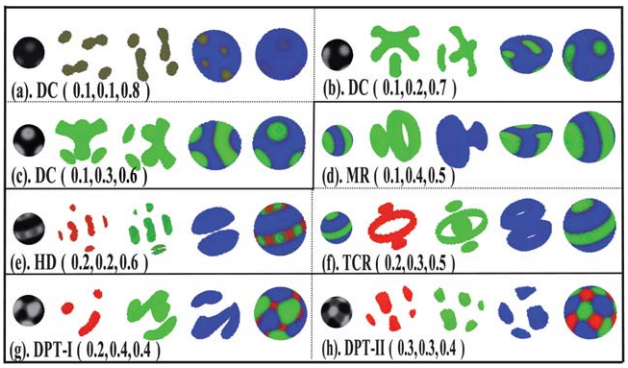

Fig. 3 Morphologies of ABC star triblock copolymers confined in a spherical cavity of diameter $d_{\text{eff}} = 7.10R_{\text{g}}$. The particle surfaces are selected to be neutral to the enclosed polymers [see eqn (15)]. The red, green and blue colors represent the A-, B- and C-rich domains, respectively. The volume fractions at which these states are stable are shown in $(f_{\text{A}}, f_{\text{B}}, f_{\text{C}})$.

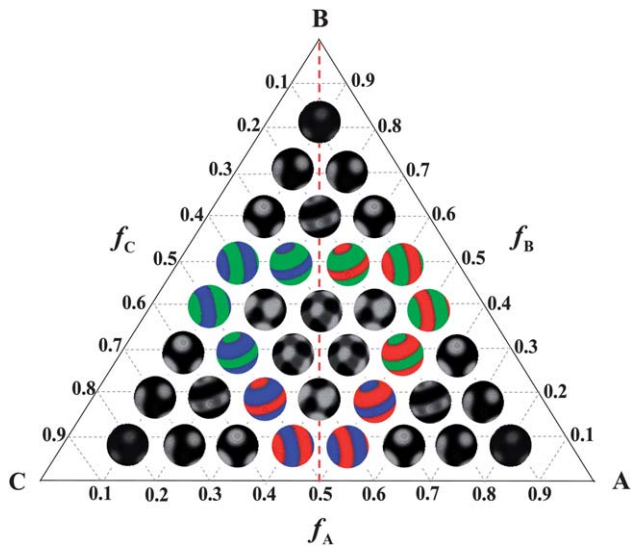

Fig. 4 Triangular phase diagram of structures in Fig. 3. The triangular phase diagram is arranged by three volume fractions $(f_{\text{A}}, f_{\text{B}}, f_{\text{C}})$. The red dashed line is the isopleth of the AC boundary.

(g) and (h): Distorted polygonal tiling (DPT) structures. These structures occur near the center of the phase diagram in Fig. 4. Two types of morphologies can be found, DPT-I and DPT-II, resembling spherical cutouts from the bulk PT [8.8.4] and PT [6.6.6] structures, respectively. Remnants of 4- and 6-fold symmetries can be viewed in these structures, as shown in Fig. 3(g) and (h). In the DPT-I structure, the polygonal cylinders are distorted to connect with each other. In comparison, in DPT-II the polygonal cylinders are kept almost unchanged from the bulk structure.

Fig. 4 is a triangular phase diagram that summarizes the morphologies and the connection between some of the structures. The overall phase diagram exhibits mirror symmetries about three isopleths because the neutral spherical surface has equal influence on the three components of the ABC star triblock copolymers. Neither spherical nor pore confinement can change the symmetry of a triangular phase diagram if a neutral surface is present; an interesting feature about the phase diagram is that the spherical confinement breaks the translational symmetries of the original bulk phases, resulting in changes in the free energy that shift the phase boundaries; the MR and TCR structures with axial symmetries are distributed in an orbicular region, as labeled by the colored phase symbols in Fig. 4. The orbicular region divides the space into two parts: the corner and central regions.

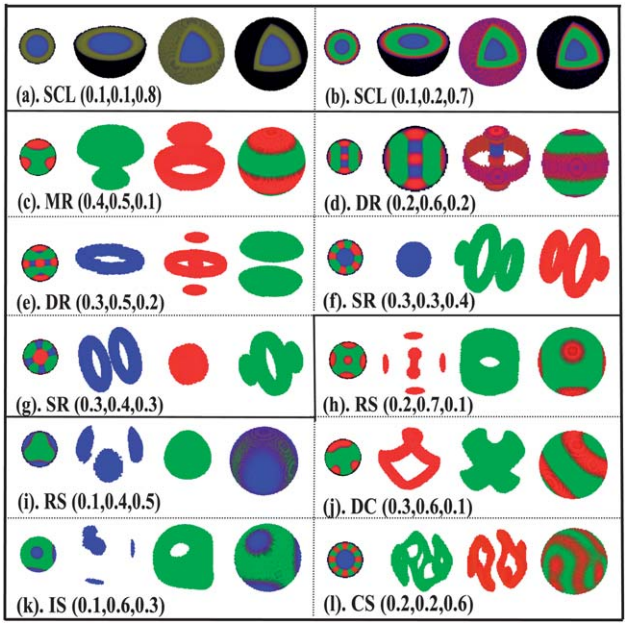

Fig. 5 Morphologies of ABC star triblock copolymers confined in a spherical cavity of diameter $d_{eff} = 7.10R_g$. The C monomers are attracted to the surface, and AB monomers are repelled from the surface [see eqn (16)]. The red, green and blue colors represent the A-, B- and C-rich domains, respectively. The volume fractions (f_A, f_B, f_C) are shown in the figure as well.

C Cavity wall that attracts one component and repels two components

In addition to the topological constraint, the short-range interaction between the boundary and copolymers induces an extra enthalpic contribution, which has been well verified to play a crucial role in the frustrated packing of block copolymers, compared to their bulk system.[40,47,48] Here, we focus on the effects of the preferential surface. While the above two sections deal with symmetric three-component systems, now we consider examples C-attractive surfaces in which one of the components adheres to the wall surface and the other two are repelled from the surface. This is realized by assuming,

$$\chi_{AW}N = \chi_{BW}N = 12 \text{ and } \chi_{CW}N = -12. \quad (16)$$

Such definition means that the spherical cavity has relatively strong adsorption effects on the C-block, comparing to the interaction parameters between the blocks (eqn (13)). In all discussion below, $d_{eff} = 7.10R_g$ is used in our numerical calculation.

Because of the rather strong wall interaction parameters and the relatively small cavity radius, the structures observed here, as shown in Fig. 5, can hardly be traced back to any bulk structures. Based on the symmetries observed in the 3D patterns, we divided these morphologies into several groups.

(a) and (b): Spherical concentric lamellae (SCL). These structures have onion-like layering systems, each layer being rich in one of the three monomer components. In Fig. 5(a), only two colors appear in the cavity except for the outermost layer; this means that the two minority blocks aggregate to the outer layers of the sphere and are well-mixed to a large degree. In Fig. 5(b), three domains are concentrically arranged from the surface to the core. This can be compared with diblock copolymers confined in a cavity reported earlier, where SCL is a direct result of either preferential surface interaction or entropic effects from the neutral confinement.[37,49] In our case, the SCL structures arise from preferential surfaces, where strong attraction between the surfaces and polymers encourages the polymers to adopt the spherical symmetry.

(c)–(g): Mushroom ring (MR), disk-ring (DR), and sphere-ring (SR) structures. The MR structure is displayed in Fig. 5(c) and is similar to that described in Section IIIB. Both DR and SR have an axial symmetry. In Fig. 5(d), the majority B-monomers form two parallel large disks and the minority A-monomers form a large ring near the surface. A- and C-rich disks appear alternately along the symmetric axis. In Fig. 5(e), DR includes a large C-rich ring, two A-rich disks, and a large B-rich ring accompanied by three B-rich disks. In Fig. 5(f), C-monomers form a spherical core and A- and B-rich regions are seen to form two rings accompanied by a small disk. In Fig. 5(g), the core region contains basically B monomers; The C-rich region forms two rings, and the A-rich region forms a large ring accompanied by two small disks.

(h)–(l): Rotational structures (RS), distorted cylinder (DC), irregular structure (IS) and complex structure (CS). RS has a rotational symmetry whereas IS is asymmetric. Fig. 5(h) and (i) show two RS structures with two block domains. In Fig. 5(h), the B-rich domains discontinuously appear in an axial symmetric form in the A-rich matrix, where the latter resembles a large cylindrical shell. In Fig. 5(i), RS includes three C-block discrete cylinders and one large B-block core. In Fig. 5(j),

two-components compete with each other; A- and B-rich regions can be best described by distorted cylinders and embed each other, which possesses a mirror symmetry. In Fig. 5(k), three irregular C-rich regions are present in a hollow B-rich structure. The CS structure in Fig. 5(l) contains the A- and B-rich distorted cylinders, which are connected and surround a C-rich spherical core.

Fig. 6 is a triangular phase diagram that summarizes the location of these morphologies. The phase diagram exhibits mirror symmetries about one isopleth only, in difference from the symmetries observed in the neutral-surface case. The preferential surface generally destroys the symmetry seen in the phase diagram of the bulk state, by frustrating the symmetric structure into a non-symmetric one; this finding was demonstrated in diblock copolymers with pore geometries.[50] In our system, the symmetries about the BC and AC isopleths disappear, as exemplified in the CS structure, with a phase point of $(f_A, f_B, f_C) = (0.2, 0.2, 0.6)$, and the DR structure, with $(f_A, f_B, f_C) = (0.2, 0.6, 0.2)$. Originally in Sections IIIA and IIIB, the structures remain unchanged when f_A and f_C are exchanged due to symmetric interactions between the three components. In the current setting, however, the surface prefers C-blocks and repels A- and B-blocks. A feature of the phase diagram is that phases with various symmetries are distributed regularly in the phase space, with a mirror symmetry about the AB isopleth. SCL structures in spherical symmetries appear in the C corner and along most points on the BC and AC lines. In these regions, SCL either experiences a strong attraction between the C-monomers and the surfaces or benefits from the "hard-wall" effects similar to those observed in diblock copolymers.[51] As expected, the SCL structure disappears along the AB line close to the A and B corners, where the RS, DC, and MR morphologies dominate. Because the C-block is very short in these regions of the parameter space ($f_C = 0.1$), the attraction becomes weak. Ring-like structures with axial symmetries, such as DR and SR, are stabilized in the central region of the parameter space. In this region, the topological constraints on the triblock copolymers are so strong that the C-attractive surface only yields the ring structure instead of SCL. A reasonable deduction is that the SR structures will maintain in the system with strong segregation when the adsorption interactions between spherical cavity walls and blocks are strong enough. Other new symmetric morphologies can be found in the parameter space due to the C-attractive surface, relative to the neutral-surface case where only axial-symmetric structures show up in an orbicular region.

D Cavity wall that attracts two components and repels one component

In this subsection, we examine yet another variation of the theme, the C-repulsive surfaces: the case of a spherical cavity that prefers the A- and B-monomers and repels C-monomers, for a fixed confinement diameter, $d_{eff} = 7.10R_g$. The interaction with the wall surface is realized by setting

$$\chi_{AW}N = \chi_{BW}N = -12 \text{ and } \chi_{CW}N = 12. \quad (17)$$

On the basis of the 3D patterns that have various symmetries, we divided these morphologies into several groups, as follows.

(a) and (b): Spherical concentric lamellae (SCL) with spherical symmetries. Two examples of SCL are illustrated in Fig. 7(a) and (b). In Fig. 7(a), SCL has a two-colored spherical lamellar structure, in which the core region contains well-mixed AB monomers. The overall structure is similar to the morphology

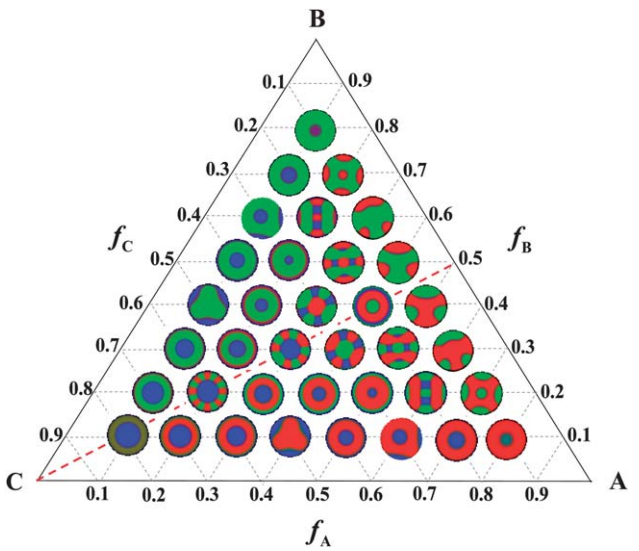

Fig. 6 Triangular phase diagrams of structures in Fig. 5. The triangular phase diagram is arranged by three volume fractions (f_A, f_B, f_C). The red dashed line is the isopleth of the AB boundary.

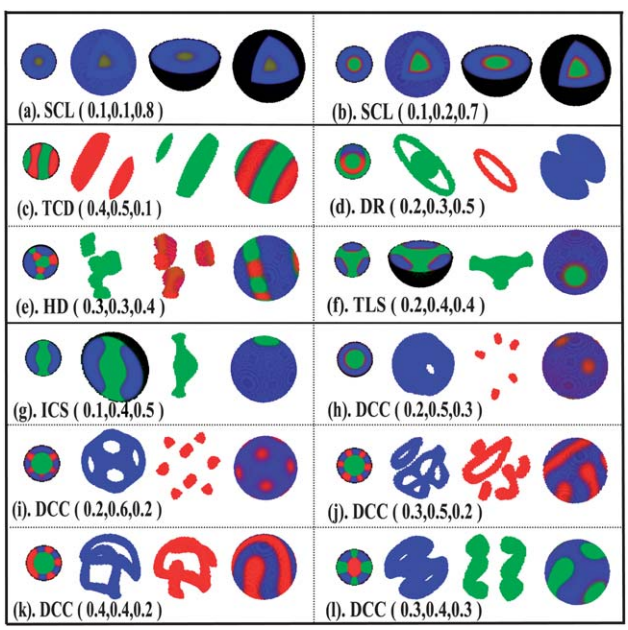

Fig. 7 Morphologies of ABC star triblock copolymers confined in a spherical cavity of diameter $d_{eff} = 7.10R_g$. The C monomers are repelled from the surface and AB monomers are attracted to the surface [see eqn (17)]. The red, green and blue colors represent the A-, B- and C- rich domains, respectively. The volume fractions (f_A, f_B, f_C) are shown in the figure as well.

illustrated in Fig. 5(a), where, however, the core region is made of C monomers. In Fig. 7(b), SCL contains three layers where the A- and B-rich domains are located in the core region and the C-rich domain is found near the surface. The layer sequence is in a reverse order to that found in Fig. 5(b), due to an interplay between confinement, entropic, and energetic preferences.

(c)–(f): Two-colored disk (TCD), disk ring (DR), hierarchical disk (HD), and triangular lamella structure (TLS). In Fig. 7(c), TCD with axial symmetry includes two block domains where A- and B-rich disks embed each other. This structure is similar to the perpendicular lamellae observed in diblock copolymer nanoparticles with neutral surfaces.[37] In Fig. 7(d), axisymmetric DR contains two C-rich disks and A- and B-rich rings. In Fig. 7(e), HD has a 4-fold rotational symmetry and features finer intervals of hierarchical disks than the other HD structure observed in Fig. 3(e). In the TLS structure shown in Fig. 7(f), the B-rich region forms a triangular domain centered in a C-rich matrix with a 3-fold rotational symmetry.

(g)–(l): Irregular cylinder structure (ICS) and distorted cylinder–core (DCC) structures. All these structures have the mirror symmetry. Among these structures, in Fig. 7(g), ICS contains a B-rich domain in an irregular cylinder form, embedded in the C-rich matrix; A series of DCC structures were observed, as shown in Fig. 7(h)–(l). These DCC structures have one spherical core in the center, and possess the mirror symmetry. In Fig. 7(h), several discrete cylinders are embedded in the C-block matrix. The DCC structure in Fig. 7(i) is similar to Fig. 7(h), because they have the similar compositions. The cylinders are distorted in DCC, as shown in Fig. 7(j)–(l).

These ordered morphologies are arranged into a triangular phase diagram shown in Fig. 8; where, the phase symbols are identical to those in Fig. 7. The SCL morphology with a spherical symmetry appears along the CB, CA, and AB lines and occupies a large space in the three triangular corners, especially in the C corner. Two other structures, ICS in Fig. 7(g) and TCD in Fig. 7(c), also appear near the mid-points of the triangle edges. Along the AB line, TCD with an axial symmetry appears next to SCL because interactions between the surface and A- or B-blocks are not weak in this parameter region. The distribution of these structures on the phase diagram suggests that in confinement, tertiary blends with one component repelling the surface are more efficient in inducing symmetric structures, in opposite to the case with two repelling components. Another feature observed is that DCC having lower symmetry appears near the center of the phase diagram, which can be compared with the system studied in Section IIIC where ring-like structures with an axial symmetry occur near the center.

E Effects of varying confinement radius and wall–polymer interaction.

In all discussion presented above, we examined a number of examples where the confinement diameter d_{eff} and the magnitude of the wall–polymer interaction $\chi_{\text{W}}N$ are fixed. Previous work demonstrated that the morphologies of diblock copolymer nanoparticles depend on the size of the confinement and property of the confining surfaces.[37–39,49] In this section, we first take a typical bulk structure, PT [6.6.6], which is stable at the center of the bulk triangle phase diagram in Fig. 2, as an example to illustrate the evolution of a number of different phases and symmetries as one of the two parameters, $\chi_{\text{W}}N$ or d_{eff}, varies. Then we draw more general conclusions.

Consider the effects caused by the magnitude of the polymer–wall interaction. In particular, we select

$$\chi_{\text{AW}}N = \chi_{\text{BW}}N = -\chi_{\text{W}}N \text{ and } \chi_{\text{CW}}N = \chi_{\text{W}}N, \quad (18)$$

where $\chi_{\text{W}}N$ is a varying parameter. The obtained morphologies are displayed in Fig. 9, where $\chi_{\text{W}}N$ increases with a step $\chi_{\text{W}}N = 4$ over a broad range. The morphology in Fig. 9(a) is the same as the one displayed in Fig. 5(f), the SR structure; this structure is stable in a particle with a strong C-attractive surface. When magnitude of $\chi_{\text{W}}N$ decreases, the original axisymmetric SR morphology undergoes a complete structural change, to a morphology that is relatively stable in a wide range of $\chi_{\text{W}}N$, as

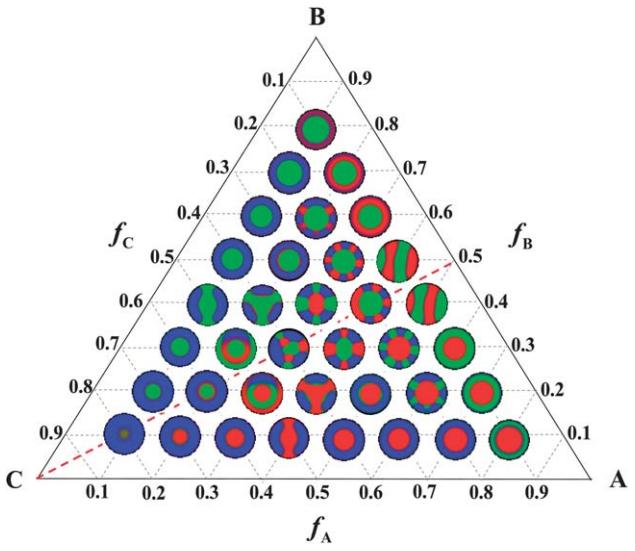

Fig. 8 Triangular phase diagrams of structures in Fig. 7. The triangular phase diagram is arranged by three volume fractions (f_A, f_B, f_C). The red dashed line is the isopleth of the AB boundary.

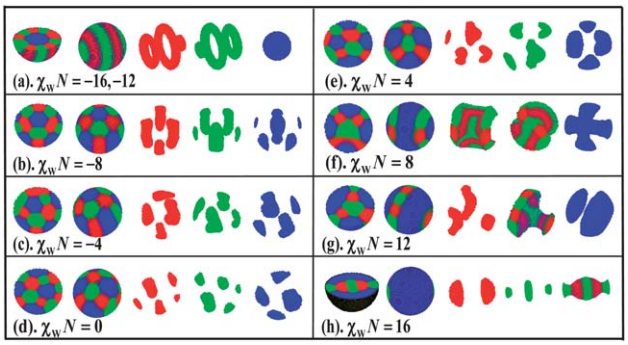

Fig. 9 Morphologies of ABC star triblock copolymers in spherical cavity as a function of degree of interaction between the polymer and wall. The red, green and blue colors represent the A-, B- and C-rich domains, respectively. The degrees of interactions $\chi_{\text{W}}N$ are also labeled below the corresponding structures.

shown in Fig. 9(b). At $\chi_W N = -4$, the structure is similar to the structure observed in the neutral surface, *i.e.*, DPT-II in Fig. 3(h), which is illustrated in Fig. 9(c) and (d). Further changing $\chi_W N$, now in the positive territory, the surface attracts two components (A and B) and repel one component (C). In the small-$\chi_W N$ range, the morphology is only gently modified from the one in the neutral surface case, as shown in Fig. 9(e). As the surface interaction increases, the morphology is obviously different from those in the small-$\chi_W N$ range, as shown in Fig. 9(f), which has a 2-fold symmetry. Then, the morphology evolves into the structure with 4-fold symmetry shown in Fig. 9(g), and into a structure with axisymmetry, as shown in Fig. 9(h). In the axisymmetric structure shown in Fig. 9(h), the surface strongly attracts A and B blocks, moving these two components to the vicinity of the surface and forming a thin AB mixed layer. Examining the change of structure as $\chi_W N$ varies, we note that the star triblocks tend to form the structures with an axisymmetry when the polymer–wall interaction is strong, either attractive or repulsive. This is different from those in diblock copolymers where the SCL structures in spherical symmetries have always been observed.[37]

Examining how the other structures evolve as the interactions change, we can draw a few general trends of structural change as the interaction varies. This can be made more explicit by examining the overall attraction, $\sum f_i \chi_{iw}$, where the summation goes over the attracted component (an equally interesting parameter can be also defined for the repulsion component). In the attraction dominating case, the concentric multi-layered structures are more stable. The observation agrees with previous studies where cylinder-forming diblock copolymers form multi-layered structures in the spherical cavity with attractive surfaces.[37,39,52] This can be understood from a simple physical picture, both in triblock and diblock copolymers: the strong attraction helps the preferred component(s) moving to the surface whereas the unpreferred component(s) moving away from the surface, forming the first few layers of an onion-like structure. In our case, the layer structures are indeed stabilized along the AB sides in the triangular phase diagram (Fig. 8), where the volume fractions are large for the preferred components, and near the C corner in the phase diagram (Fig. 6 and 8), where the volume fraction is large for the C component. In Sections IIIC and IIID, more SCL structures appear in the C-repulsive surface case than those in the C-attractive surface case, because the wall attracts two blocks in the former case while only attracts one block in the latter case. This fact further supports the notion that the overall strong attraction prefers more SCL in the phase diagrams. We expect that this trend is general, even systems with parameters beyond those examined here.

Now, we consider an example which demonstrates the confinement-dimension effects. Taking the neutral surface as an example, we consider the range of variation, $d_{\text{eff}} = 3.52R_g$ to $9.16R_g$. The series of morphologies are shown in Fig. 10. In Fig. 10(a), in a strong confinement, DPTa is a discrete structure where two majority-block domains surround a minority-block along the x-axis. This structure has a 2-fold rotational symmetry along the x direction, and is stable within the range $d_{\text{eff}} = 3.52R_g$ to $4.11R_g$. In Fig. 10(b), another type of structure, DPTb, arises in

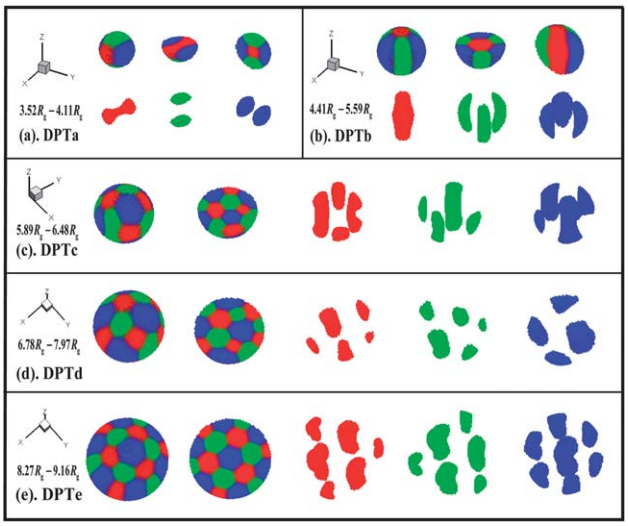

Fig. 10 Morphologies of ABC star triblock copolymers in a spherical cavity as a function of confining diameter. A neutral wall, eqn (15) is assumed. The red, green and blue colors represent the A-, B- and C-rich domains, respectively. The phases are also labeled below the corresponding structures.

the parameter range $d_{\text{eff}} = 4.41R_g$ to $5.59R_g$; the majority blocks form three distorted cylinders and the minority block forms one cylinder at the center. This structure also possesses a 3-fold rotational symmetry about the z-axis. Irregular discrete structures were observed in diblock nanoparticles where the diameters are smaller than the corresponding bulk periods.[49] In the current system, a strong confinement prefers structure with rotational symmetries. Note that the unit cell of the bulk PT structure has a size of $L_1 \approx L_2 \approx 4.00R_g$ (see Table 1). The range of d_{eff} used in these calculations is comparable to the unit-cell size, hence completely destroying the original PT period structure.

Within the next range, d_{eff} from $5.89R_g$ to $7.97R_g$, the confinement diameter is somewhat greater than the original PT unit-cell size. Two distinct morphologies were found and shown in Fig. 10(c) and (d). The arrangement of the majority and minority blocks starts to show patterns that are similar to the arrangement in the bulk PT structure, with a spherical cutout. The confinement entropy now dominates the variation of the structures, which distorts PT near the spherical boundary. No rotational symmetry can be detected in this intermediate d_{eff} range. In the large confinement range $d_{\text{eff}} > 8.27R_g$, as shown in Fig. 10(e), structures with a 6-fold rotational symmetry and cylinder-like domains start to emerge. The system now has some characteristics of the bulk PT structure, except for the translational symmetry along the z-axis.

In order to show that the structures illustrated in Fig. 10 are indeed distinct from each other, we depict the dependence of the free-energy difference $\Delta F/nk_BT$ as a function of d_{eff}/R_g in Fig. 11, where $\Delta F = F - F_{\text{bulk}}$ and $F_{\text{bulk}}/nk_BT = 9.9343$ is the bulk free energy per chain in units of k_BT. The five free-energy branches, each corresponding to a structure in Fig. 9, can be viewed here. The crossing points determine the first-order phase transitions between the five studied phases. We have no

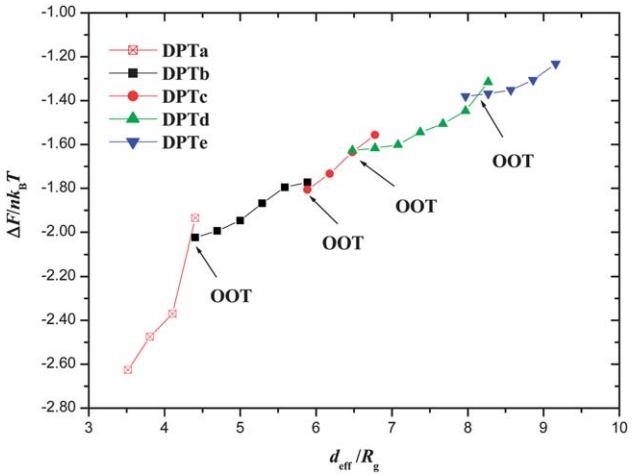

Fig. 11 The free energy curves for the five morphologies in Fig. 9. The order–order transition points are denoted as OOT.

additional data for the region beyond $d_{eff} > 9.3R_g$, as the computed system reaches the limit of the current computational capability. We expect more stages of structural transitions; each stage favors a particular surface arrangement that distort the pattern of a bulk structure. The plots in Fig. 11 show that as d_{eff} grows, the free-energy variation of higher energy branch starts to become more flat, which is a reflection of the fact that the interior of the confined structure now resembles that in a bulk phase, dominating the free energy behavior. A general expectation of any confinement system is that as the confinement diameter d_{eff} grows, the system appears more similar and finally converges to the bulk structure; this is true for all structures examined here.

IV Conclusions

We performed a self-consistent field theory study on the morphologies and phase diagrams of symmetric ABC star triblock copolymer nanoparticles using the pseudospectral method in an implementation suitable for parallel computation. The structure distributions were illustrated in the triangular phase diagrams for each example case by varying the volume fractions of the system in an increment of 0.1. In the first case (Section IIIB), we considered a confinement environment that has a neutral interaction with the enclosed polymers; in the second and third cases (Sections IIIC and IIID), we considered a confinement surface that may have different degrees of preferential interactions with the enclosed polymers. Finally, using a small increment, we demonstrate the stability of a series of structures having distinct spatial symmetries, associated with a changing confinement radius and a varying degree of interactions between the polymer and wall, for a particular bulk structure.

A general feature of the calculated phase diagrams is the shift of the original phase boundaries in a bulk system and creation of new structures particular to confined systems. For example, the original bulk PT [6.6.6] has a 6-fold cylinder symmetry, but, in confinement, it could display a new conformation such as the ring-like structure, which can conveniently fit inside the sphere and has no relation with the original structure, in a cavity with an AB-repulsive and C-attractive surface, as shown in Fig. 5(f) and (g). Another general feature is that the phases in the centre of phase diagrams have different behavior from those in the corners of phase diagrams. The former exhibits translational symmetry due to the star topological constraint, while the latter has similar behavior as those in diblock copolymers. Systems belong to the corner of phase diagram can easily assemble into SCL structures, which are commonly observed in the diblock copolymers. In contrast, the system favors SR phases in the central region of the phase diagram, even with a strongly attractive surface, because of the translational symmetry from the star topology.

In summary, due to the special architecture of the polymer chains and the spherical confinement adopted, a rich variety of three-dimensional morphologies in various symmetries were observed when the system is considered under different physical conditions; some of the structural patterns are observed for the first time, further enriching the existing structural library for block copolymer nanoparticles. In view of potential applications of block-copolymer nanoparticles, the theoretical prediction in this work gives guidance to synthesizing practically useful nano-sized materials.

Acknowledgements

We thank for the financial supports from the National Natural Science Foundation of China (no. 21074096 and 21204067), and the Natural Science and Engineering Research Council of Canada. Y. J. thanks the startup funding from Wenzhou University. We also thank SHARCNET for providing computation time.

References

1 H. Otsuka, Y. Nagasaki and K. Kataoka, *Adv. Drug Delivery Rev.*, 2003, **55**, 403.
2 H. H. Pham, I. Gourevich, J. K. Oh, J. E. N. Jonkman and E. Kumacheva, *Adv. Mater.*, 2004, **16**, 516.
3 I. Gourevich, L. M. Field, Z. Wei, C. Paquet, A. Petukhova, A. Alteheld, E. Kumacheva, J. J. Saarinen and J. E. Sipe, *Macromolecules*, 2006, **39**, 1449.
4 S. Zhang, K. H. Chan, R. K. Prud'homme and A. J. Link, *Mol. Pharmaceutics*, 2012, **9**, 2228.
5 I. Wyman, G. Njikang and G. Liu, *Prog. Polym. Sci.*, 2011, **36**, 1152.
6 A.-C. Shi and B. Li, *Soft Matter*, 2013, **9**, 1398.
7 T. Gemma, A. Hatano and T. Dotera, *Macromolecules*, 2002, **35**, 3225.
8 Y. Matsushita, *Macromolecules*, 2007, **40**, 771.
9 S. Sioula, N. Hadjichristidis and E. L. Thomas, *Macromolecules*, 1998, **31**, 8429.
10 H. Hückstädt, A. Gopfert and V. Abetz, *Macromol. Chem. Phys.*, 2000, **201**, 296.

11 K. Yamauchi, K. Takahashi, H. Hasegawa, H. Iatrou, N. Hadjichirstidis, T. Kaneko, Y. Nishikawa, H. Jinnai, T. Matsui, H. Nishioka, M. Shimizu and H. Furukawa, *Macromolecules*, 2003, **36**, 6962.
12 A. Takano, S. Wada, S. Sato, T. Araki, K. Hirahara, T. Kazama, S. Kawahara, Y. Isono, A. Ohno, N. Tanaka and Y. Matsushita, *Macromolecules*, 2004, **37**, 9941.
13 K. Yamauchi, S. Akasaka, H. Hasegawa, H. Iatrou and N. Hadjichristidis, *Macromolecules*, 2005, **38**, 8022.
14 A. Takano, W. Kawashima, A. Noro, Y. Isono, N. Tanaka, T. Dotera and Y. Matsushita, *J. Polym. Sci., Part B: Polym. Phys.*, 2005, **43**, 2427.
15 K. Hayashida, W. Kawashima, A. Takano, Y. Shinohara, Y. Amemiya, Y. Nozue and Y. Matsushita, *Macromolecules*, 2006, **39**, 4869.
16 K. Hayashida, A. Takano, S. Arai, Y. Shinohara, Y. Amemiya and Y. Matsushita, *Macromolecules*, 2006, **39**, 9402.
17 K. Hayashida, T. Dotera, A. Takano and Y. Matsushita, *Phys. Rev. Lett.*, 2007, **98**, 195502.
18 G. H. Fredrickson, V. Ganesan and F. Drolet, *Macromolecules*, 2002, **35**, 16.
19 X. He, L. Huang, H. Liang and C. Pan, *J. Chem. Phys.*, 2002, **116**, 10508.
20 P. Tang, F. Qiu, H. Zhang and Y. Yang, *J. Phys. Chem. B*, 2004, **108**, 8434.
21 C.-I. Huang, H.-K. Fang and C.-H. Lin, *Phys. Rev. E: Stat., Nonlinear, Soft Matter Phys.*, 2008, **77**, 031804.
22 W. Li, Y. Xu, G. Zhang, F. Qiu, Y. Yang and A.-C. Shi, *J. Chem. Phys.*, 2010, **133**, 064904.
23 G. Zhang, F. Qiu, H. Zhang, Y. Yang and A.-C. Shi, *Macromolecules*, 2010, **43**, 2981.
24 K. Hayashida, N. Saito, S. Arai, A. Takano, N. Tanaka and Y. Matsushita, *Macromolecules*, 2007, **40**, 3695.
25 Y. Xu, W. Li, F. Qiu, H. Zhang, Y. Yang and A.-C. Shi, *J. Polym. Sci., Part B: Polym. Phys.*, 2010, **48**, 1101.
26 C. R. Stewart-Sloan and E. L. Thomas, *Eur. Polym. J.*, 2011, **47**, 630.
27 P. Romiszowski and A. Sikorski, *J. Chem. Phys.*, 2002, **116**, 1731.
28 J. R. Maury-Evertsz, L. A. Estevez and G. E. Lopez, *J. Chem. Phys.*, 2004, **121**, 8652.
29 A. Sikorski and P. Romiszowski, *J. Chem. Phys.*, 2004, **120**, 7206.
30 P. Romiszowski and A. Sikorski, *J. Chem. Phys.*, 2005, **123**, 104905.
31 P. Romiszowski and A. Sikorski, *J. Math. Chem.*, 2006, **40**, 295.
32 W. Han, P. Tang, X. Li, F. Qiu, H. Zhang and Y. Yang, *J. Phys. Chem. B*, 2008, **112**, 13738.
33 B. Lin, H. Zhang, F. Qiu and Y. Yang, *Langmuir*, 2010, **26**, 19033.
34 Y. Xu, W. Li, F. Qiu and Y. Yang, *J. Phys. Chem. B*, 2009, **113**, 11153.
35 J. Song, T. Shi, J. Chen and L. An, *J. Phys. Chem. B*, 2010, **114**, 16318.
36 S. Li, W. Qiu, L. Zhang and H. Liang, *J. Chem. Phys.*, 2012, **136**, 124906.
37 B. Yu, B. Li, Q. Jin, D. Ding and A.-C. Shi, *Macromolecules*, 2007, **40**, 9133.
38 T. Higuchi, A. Tajima, K. Motoyoshi, H. Yabu and M. Shimomura, *Angew. Chem., Int. Ed.*, 2008, **47**, 8044.
39 P. Chen, H. Liang and A.-C. Shi, *Macromolecules*, 2008, **41**, 8938.
40 V. Khanna, E. W. Cochran, A. Hexemer, G. E. Stein, G. H. Fredrickson, E. J. Kramer, X. Li, J. Wang and S. F. Hahn, *Macromolecules*, 2006, **39**, 9346.
41 G. H. Fredrickson, *The Equilibrium Theory of Inhomogeneous Polymers*, Oxford University Press, Oxford, UK, 2006.
42 G. Tzeremes, K. O. Rasmussen, T. Lookman and A. Saxena, *Phys. Rev. E: Stat., Nonlinear, Soft Matter Phys.*, 2002, **65**, 041806.
43 F. Drolet and G. H. Fredrickson, *Phys. Rev. Lett.*, 1999, **83**, 4317.
44 S. W. Sides and G. H. Fredrickson, *Polymer*, 2003, **44**, 5859.
45 P. Tang, F. Qiu, H. Zhang and Y. Yang, *Phys. Rev. E: Stat., Nonlinear, Soft Matter Phys.*, 2004, **69**, 031803.
46 Z. Guo, G. Zhang, F. Qiu, H. Zhang and Y. Yang, *Phys. Rev. Lett.*, 2008, **101**, 028301.
47 M. W. Matsen, *J. Chem. Phys.*, 1997, **106**, 7781.
48 W. Li and R. A. Wickham, *Macromolecules*, 2009, **42**, 7530.
49 S. Li, P. Chen, L. Zhang and H. Liang, *Langmuir*, 2011, **27**, 5081.
50 W. Li, R. A. Wickham and R. A. Garbary, *Macromolecules*, 2006, **39**, 806.
51 D. Meng and Q. Wang, *J. Chem. Phys.*, 2007, **126**, 234902.
52 B. Yu, B. Li, Q. Jin, D. Ding and A. -C. Shi, *Soft Matter*, 2011, **7**, 10227.

